

Computational temporal ghost imaging based on complementary modulation

Jia-Wei Li(李佳炜), Wei Zhang(张伟), Xue-Feng Liu(刘雪峰), and Xu-Ri Yao(姚旭日)

Citation: Chin. Phys. B, 2024, 33 (**11**): 114201. DOI: 10.1088/1674-1056/ad74e8
Journal homepage: http://cpb.iphy.ac.cn; http://iopscience.iop.org/cpb

What follows is a list of articles you may be interested in

Image encryption algorithm based on multiple chaotic systems and improved Joseph block scrambling

Dingkang Mou(牟定康) and Yumin Dong(董玉民)
Chin. Phys. B, 2024, 33 (**10**): 104205. DOI: 10.1088/1674-1056/ad6257

High-quality ghost imaging based on undersampled natural-order Hadamard source

Kang Liu(刘炕), Cheng Zhou(周成), Jipeng Huang(黄继鹏), Hongwu Qin(秦宏伍), Xuan Liu(刘轩), Xinwei Li(李鑫伟), and Lijun Song(宋立军)
Chin. Phys. B, 2024, 33 (**9**): 094204. DOI: 10.1088/1674-1056/ad62e1

Optical encryption scheme based on spread spectrum ghost imaging

Jin-Fen Liu(刘进芬), Yue Dong(董玥), Le Wang(王乐), and Sheng-Mei Zhao(赵生妹)
Chin. Phys. B, 2023, 32 (**7**): 074202. DOI: 10.1088/1674-1056/acbf27

A probability theory for filtered ghost imaging

Zhong-Yuan Liu(刘忠源), Shao-Ying Meng(孟少英), and Xi-Hao Chen(陈希浩)
Chin. Phys. B, 2023, 32 (**4**): 044204. DOI: 10.1088/1674-1056/ac981e

Ghost imaging based on the control of light source bandwidth

Zhao-Qi Liu(刘兆骐), Yan-Feng Bai(白艳锋), Xuan-Peng-Fan Zou(邹璇彭凡), Li-Yu Zhou(周立宇), Qin Fu(付芹), and Xi-Quan Fu(傅喜泉)
Chin. Phys. B, 2023, 32 (**3**): 034210. DOI: 10.1088/1674-1056/ac6edd

---

Computational temporal ghost imaging based on complementary modulation

Jia-Wei Li(李佳炜)[1], Wei Zhang(张伟)[1], Xue-Feng Liu(刘雪峰)[2,3,†], and Xu-Ri Yao(姚旭日)[1‡]

[1] *Center for Quantum Technology Research and Key Laboratory of Advanced Optoelectronic Quantum Architecture and Measurements (MOE) School of Physics, Beijing Institute of Technology, Beijing* 100081, *China*

[2] *Key Laboratory of Electronics and Information Technology for Space Systems, National Space Science Center, Chinese Academy of Sciences, Beijing* 100190, *China*

[3] *University of Chinese Academy of Sciences, Beijing* 100049, *China*

(Received 10 July 2024; revised manuscript received 21 August 2024; accepted manuscript online 29 August 2024)

We report an experimental demonstration of temporal ghost imaging in which a digital micromirror device (DMD) and $+1/-1$ binary modulation have been combined to give an accurate reconstruction of a nonperiodic time object. Compared to the $0/1$ modulation, the reconstruction signal can be improved greatly by $+1/-1$ binary modulation even with half of the measurements. Experimental results show that $0/1$ binary temporal objects up to 4 kHz and sinusoidal time objects up to 1 kHz can be reconstructed by this method. The influences of modulation speed and array detector gray levels are also discussed.

Keywords: temporal ghost imaging, complementary modulation

PACS: 42.30.Va, 42.30.Ms **DOI:** 10.1088/1674-1056/ad74e8

1. Introduction

Ghost imaging (GI) is an imaging technique that employs a bucket detector, devoid of spatial resolution, to collect light emitted or reflected by an object. Simultaneously, it utilizes another detector with spatial resolution to accurately measure information pertaining to the light source. Image of the object can be obtained from the second-order correlation of signals on the detectors.[1–5] GI shows superiorities to the traditional imaging due to its features such as free from the atmospheric disturbance[6,7] and lensless imaging.[4,5,8,9] These advantages make GI important and practical in real applications in the wide range of areas.[10–14]

The concept of GI has been extended from spatial imaging to time domain in recent years, in which a temporal signal can be reconstructed with a detector that is much slower. In 2010, Shirai *et al.* theoretically demonstrated the feasibility of temporal GI (TGI) by utilizing classical unsteady light sources.[15] In 2012, Chao *et al.* verified the viability of TGI through simulation.[16] In 2016, Ryczkowski *et al.* experimentally achieved TGI for the first time.[17] Various modulations and recovery algorithms have been proposed to improve the reconstruction quality.[18–24] The GI correlation algorithm needs mounts of number of measurements to enhance the signal-to-noise ratio (SNR) of the retrieved signal, and periodic temporal objects were employed in the TGI demonstrations above. In 2016, Devaux *et al.* proposed a single-shot time-domain computational GI scheme by performing spatial multiplexing measurement, in which random images displayed by a liquid crystal display (LCD) and the images, modulated by a temporal signal, recorded, and summed on a chip complementary metal oxide semiconductor (CMOS) camera are utilized to obtain a nonreproducible time object.[25] Temporal resolution and SNR which strongly relates to the number of measurements determine the performance of TGI system. In the single-shot TGI configuration above, the temporal resolution and the number of the measurements corresponds to the displaying speed and pixel number of the LCD, respectively.

In this paper, we employ $+1/-1$ binary patterns and digital micromirror device (DMD) to achieve a nonperiodic time signal reconstruction. The $+1/-1$ binary patterns have been demonstrated to have a better performance than the $0/1$ binary patterns.[26] DMD consists of an array of individually addressable mirrors and each mirror can be tilted in two different directions with respect to the surface of the DMD. The flipping speed of the micromirror is up to tens of kilohertz which is faster than the LCD displaying frame rate. Since only nonnegative matrices can be physically displayed by DMD, the $+1/-1$ binary pattern is realized by displaying a $0/1$ pattern with its inverse side by side. Experimental results show that the restored signal quality can be improved greatly by $+1/-1$ binary patterns compared to the $0/1$ binary patterns, although the measurements for $+1/-1$ binary modulation are half of that for $0/1$ binary modulation. A nonperiodic binary signal with a frequency up to 4 kHz can be reconstructed with $+1/-1$ binary modulation, while bit error may appear in the reconstructed 1 kHz signal under the conventional $0/1$ binary

†Corresponding author. E-mail: liuxuefeng@nssc.ac.cn
‡Corresponding author. E-mail: yaoxuri@bit.edu.cn

© 2024 Chinese Physical Society and IOP Publishing Ltd

modulation. Another experiment was performed with a light chopper to reconstruct sinusoidal signals. The influence of detector gray levels and modulation speed on the reconstructed signal quality are analyzed.

2. Scheme and experimental setup

The experimental setup is schematically illustrated in Fig. 1. In the signal generation part, the light from a tungsten-halogen light source (Thorlabs SLS201/M) irradiated the plane of DMD1 after it collimated and broadened. DMD1 (JinHuaFeiGuang F6500) includes 1920×1080 micromirrors, and each micromirror is 7.56 μm × 7.56 μm in size. In the signal generation process, a sequential $0/1$ binary signal was encoded on the DMD1 and all the micromirrors of DMD1 flipped consistently according to the signal (directions $+12°$ (1) and $-12°$ (0)). The temporal binary light signal can be obtained from direction $+12°$ of DMD1.

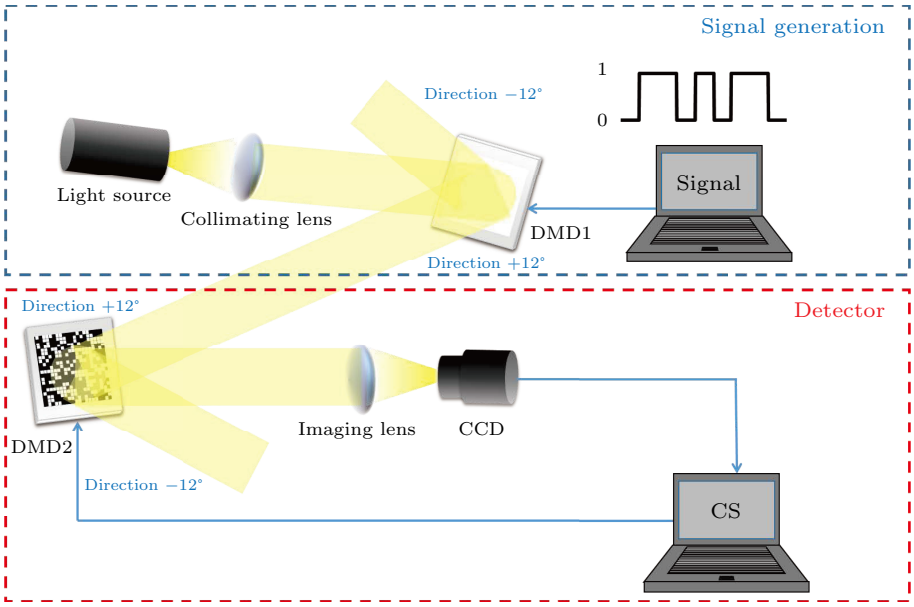


Fig. 1. Experimental setup for computational TGI based on complementary modulation.

In the detector part, DMD2 (TI DLP7500) contains 1024×768 micromirrors with a size of 13.68 μm × 13.68 μm, and has a maximum mirror flipping frame rate 20 kHz. The output light from the signal generation part illuminated in the direction $+12°$ of DMD2, and an area on the DMD2 in the window of size 512×512 micromirrors was employed to provide binary intensity modulation. In the experiment, the binary pattern was realized by group clusters of 8×8 mirrors, so the actual size of the modulation pixel was 109.44×109.44 μm, and 512×512 micromirrors corresponded to 64×64 modulation pixels. A charge coupled device (CCD, IMPERX B1620M) with a 1680×1024 pixel array and pixel size of 7.40 μm × 7.40 μm was placed in front of DMD2. The modulation area of DMD2 was imaged onto a 960×960 pixels region of interest (ROI) on the CCD by an imaging lens. Thus one modulation pixel on the DMD2 corresponded to a 15×15 pixels region on the CCD, and only the intensities of the pixel in the center of this region were utilized in the experiments to obtain a 64×64 measurement matrix. The crosstalk at the edges in the binary patterns was avoided. In the GI performing with DMD, $+1/-1$ binary modulation is achieved by displaying $0/1$ pattern followed immediately by its inverse, and subtracting two measurements sequentially. In TGI, twice modulations will lead to a decrease of temporal resolution. In this experiment, as shown in Fig. 2, a 64×32 random 1/0 pattern was generated beforehand, then every column of this pattern was inserted with its inverse by side, and the previous 1/0 pattern was extended to a 64×64 1/0 pattern. The measurements of $+1/-1$ modulation were obtained from the deduction of odd and even columns in a measurement matrix.

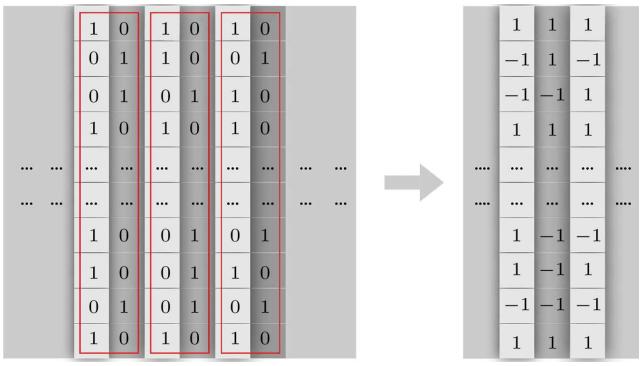


Fig. 2. The implementation of $+1/-1$ modulation.

The time object $X(t)$ was a randomly generated sequence of 1 and 0 and generated on DMD1. A measurement matrix

recorded by CCD is

$$I_{ij} = \int X(t) P_{m,ij} \mathrm{d}t, \tag{1}$$

where $P_{m,ij}$ is the m-th pattern encoded to DMD2, i and j are coordinates of the pattern. As mentioned above, the $+1/-1$ modulation measurement is

$$I'_{ij} = I^{\mathrm{O}}_{ij} - I^{\mathrm{E}}_{ij}, \tag{2}$$

where I^{O}_{ij} and I^{E}_{ij} are odd and even columns of I_{ij}, respectively. Similarly, the $+1/-1$ modulation pattern is

$$P'_{m,ij} = P^{\mathrm{O}}_{m,ij} - P^{\mathrm{E}}_{m,ij}, \tag{3}$$

where $P^{\mathrm{O}}_{m,ij}$ and $P^{\mathrm{E}}_{m,ij}$ are odd and even columns of $P_{m,ij}$, respectively. Compressive sensing (CS) algorithm was employed in the experiments to reconstruct the time object information.[27,28]

$$X'(t) = \arg\min \left\{ \left\| \int X'(t) P'_{m,ij} \mathrm{d}t - I'_{ij} \right\|_2^2 + \tau \left\| X'(t) \right\|_1 \right\}, \tag{4}$$

where $X'(t)$ is the reconstructed time object and τ is a constant scalar weighting the relative strength of the two terms. TVAL3 (total variation augmented lagrangian alternating direction algorithm) algorithm[29] was utilized to solve the optimization problem specified by Eq. (4):

$$X'(t) = \arg\min \left\{ \left\| \int X'(t) P'_{m,ij} \mathrm{d}t - I'_{ij} \right\|_2^2 + \tau \left\| \mathrm{TV}(X'(t)) \right\| \right\}, \tag{5}$$

where $\|\mathrm{TV}(\mathrm{X}'(\mathrm{t}))\| = \|\boldsymbol{D}(X'(t))\|_1$, and $\boldsymbol{D}$ is the one-dimensional differential operation.

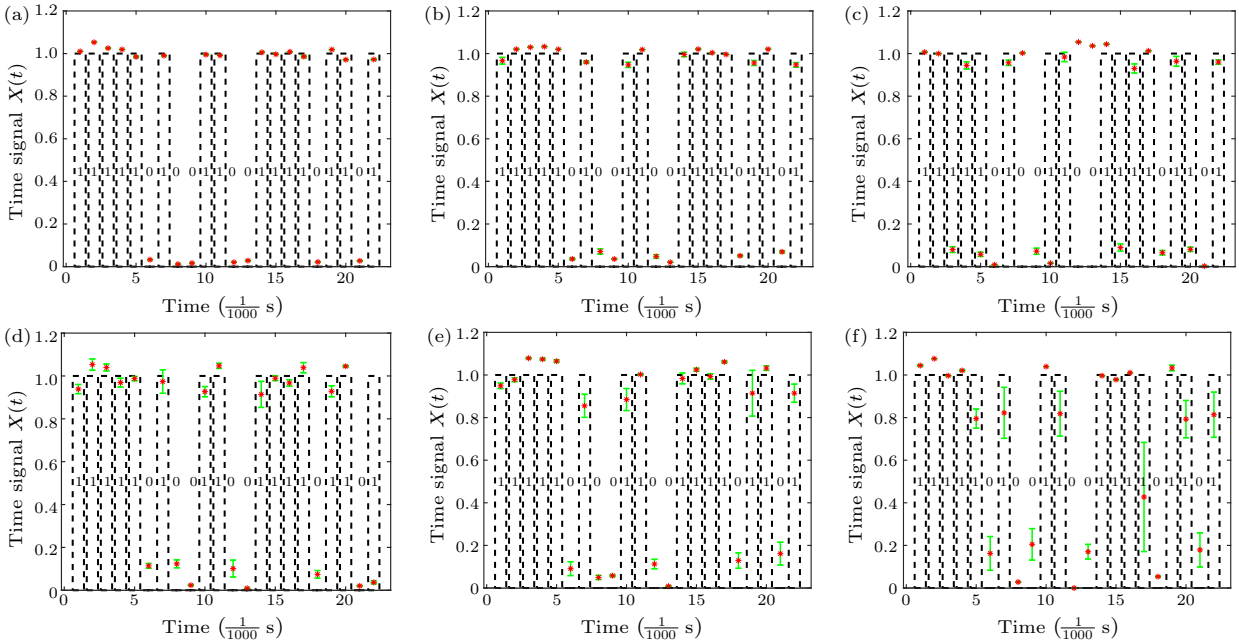


Fig. 3. Experimental results of 1 kHz 0/1 binary time object. The dotted lines are the original 0/1 time objects, and the red asterisks are the recovered data. There are 22 bits of the object and reconstructions that were selected for demonstration. (a)–(c) The results under modulation speeds of 5 kHz, 4 kHz, and 3 kHz with $+1/-1$ patterns, respectively. (d)–(f) The results under modulation speeds of 5 kHz, 4 kHz, and 3 kHz with 0/1 patterns, respectively.

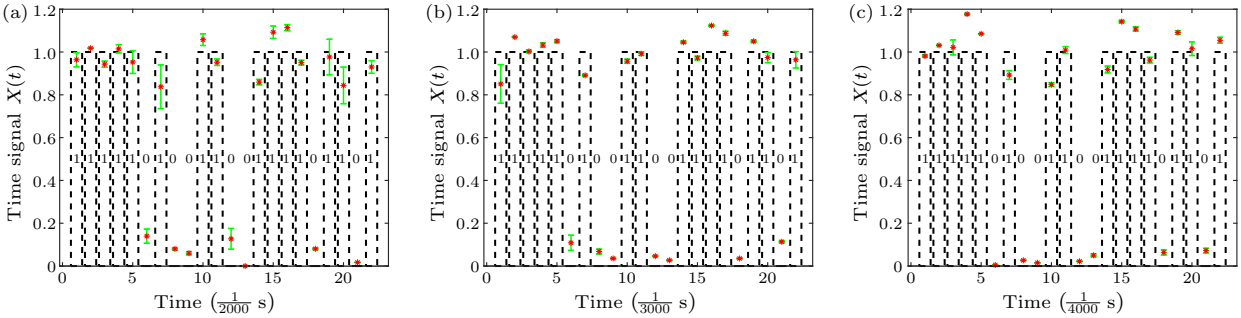


Fig. 4. (a)–(c) The recoveries of 2 kHz, 3 kHz, and 4 kHz time objects, respectively, under the conditions that the frequencies of modulation were 3 times of objects.

3. Experimental results

In the 0/1 binary signal reconstruction experiments, a random 0/1 binary signal of 300 bits was generated and displayed in a frequency range from 1 kHz to 4 kHz. The exposure time of the CCD was 0.285 s. The reconstructions of 1 kHz signal under modulation speeds of 5 kHz, 4 kHz,

and 3 kHz are shown in Figs. 3(a)–3(c), respectively. The signal reconstructed from 5 kHz modulation gives better performance. To make a comparison, $0/1$ binary modulation experiments were performed, in which random $0/1$ binary patterns with a size of 64×64 were loaded on DMD2. The number of measurements of $0/1$ modulation was $64 \times 64 = 4096$, while that of $+1/-1$ modulation was $64 \times 32 = 2048$. The results of $0/1$ modulation are shown in Figs. 3(d)–3(f). It is shown that, with $+1/-1$ modulation, the signal quality can be improved greatly even at a low sampling rate. Notice the error bar in Fig. 3(f), it can be seen that bit error may appear in the reconstructions of $0/1$ binary time object from $0/1$ binary modulation. The $+1/-1$ binary modulation yields reliable results in the 4 kHz signal recovery experiment. The recoveries of 2 kHz, 3 kHz, and 4 kHz time objects are shown in Figs. 4(a)–4(c), respectively, under the conditions the frequencies of modulation were 3 times of objects. The selection of modulation frequencies will be analyzed in the following.

We also tested this TGI method with sinusoidal temporal signals. As shown in Fig. 5, sinusoidal temporal signals were produced by an optical chopper (OCV-6300F). The equipment in detector and experimental parameters were the same as those in the $0/1$ binary signal reconstruction experiments. The frequency of modulation was 5 times that of the object. The results of sinusoidal temporal signals with frequencies 100 Hz, 500 Hz and 1 kHz are shown in Figs. 6(a)–6(c), respectively. The original sinusoidal temporal signals were recorded by a fast detector and are indicated by red lines in Fig. 6. The experimental results show that signal waveforms can effectively be recovered from this TGI method.

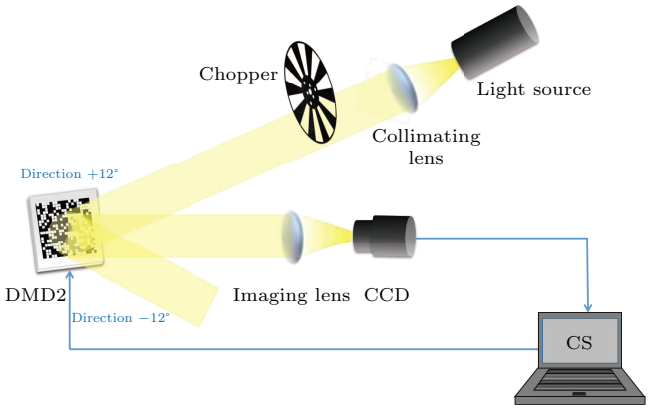


Fig. 5. Experimental setup for sinusoidal temporal signals.

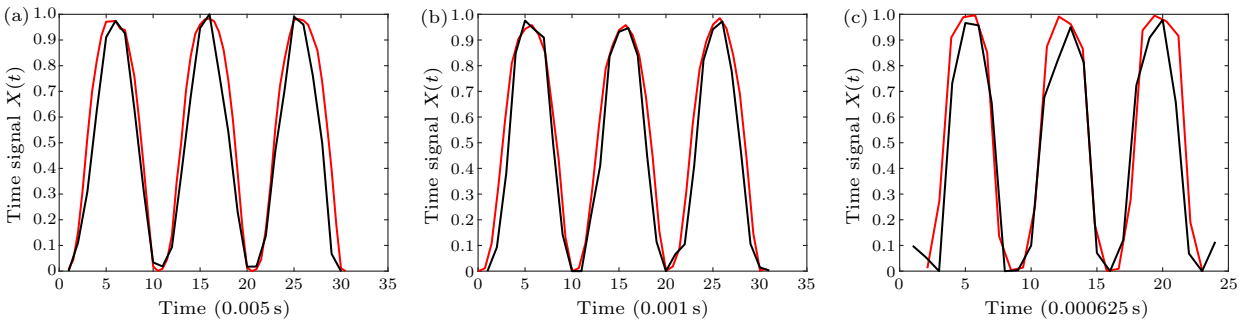


Fig. 6. Experimental results for sinusoidal temporal signals with frequencies (a) 100 Hz, (b) 500 Hz and (c) 1 kHz. Red lines are the records from a fast detector and the black lines are TGI reconstructions.

4. Modulation frequency

According to the Shannon–Nyquist sampling theorem which specifies that one must sample at least two times faster than the signal bandwidth when capturing a signal, the modulation frequency should be at least twice the maximum frequency of a nonsynchronizable time object. Generally, a higher sampling frequency brings a better acquisition of signal. However, we find that the rising of modulation frequency may introduce an adverse impact to this single-shot TGI system.

We use F_{X} to denote the maximum frequency of the object, and F_{M} to denote the modulation frequency. If the object is an N-dimensional vector, then the reconstructed signal is $F_{\mathrm{M}}/F_{\mathrm{X}} \cdot N$-dimensional vector. The sampling rate is defined as

$$(F_{\mathrm{M}}/F_{\mathrm{X}} \cdot N)/M, \tag{6}$$

where M is the number of measurements. In this single-shot TGI configuration, M is defined by the pixel number of the detector, which cannot be increased infinitely. Thus, from the view of CS reconstruction, the increase of the modulation frequency will lead to a decrease of the sampling rate, and a reduction in the recovery quality. The increase of the modulation frequency also requires a higher dynamic range of the detector.

Experiments were carried out to demonstrate the relation between the modulation frequency and recovery quality. Peak signal-to-noise ratio (PSNR) reads

$$\mathrm{PSNR} = 10 \times \log_{10}\left(\frac{\mathrm{peakval}^2}{\mathrm{MSE}}\right), \tag{7}$$

where peakval is the maximum intensity of the signal, and MSE is the mean square error expressed as

$$\mathrm{MSE} = \frac{1}{N}\sum_{t}[X(t) - X'(t)]^2, \tag{8}$$

where $X'(t)$ was reshaped to an N-dimensional vector by averaging intervals of $F_{\mathrm{M}}/F_{\mathrm{X}}$ elements sequentially. Equation (7)

was employed to provide a quantitative comparison of the recovery quality. The time object was a 2 kHz random $0/1$ binary signal of 30 bits. The experimental situations were same as the $0/1$ binary signal reconstruction experiments mentioned above. The reconstructions without normalization under modulation frequencies from 4 kHz to 14 kHz are shown in Figs. 7(a)–7(f), respectively. The lengthes of reconstructed signal increase with the rising modulation frequency, while the intensities of the signals descend. The reconstructed signals were approximately normalized to $[0, 1]$, and the curve of PSNR versus modulation frequency is shown in Fig. 8. We find that the the recovery quality becomes better in the initial stage and then gets worse with the increase of modulation frequency. To a 2 kHz $0/1$ binary signal, the best value of $F_{\mathrm{M}}/F_{\mathrm{X}}$ is 3 in this experiment. Generally, the PSNR was found to reach its maximum with an $F_{\mathrm{M}}/F_{\mathrm{X}}$ of 3 or 4 in this experiment, and as shown in Fig. 4, the value $F_{\mathrm{M}}/F_{\mathrm{X}} = 3$ was used in the experiments above. The best value of $F_{\mathrm{M}}/F_{\mathrm{X}}$ depends experimental conditions and requires further research.

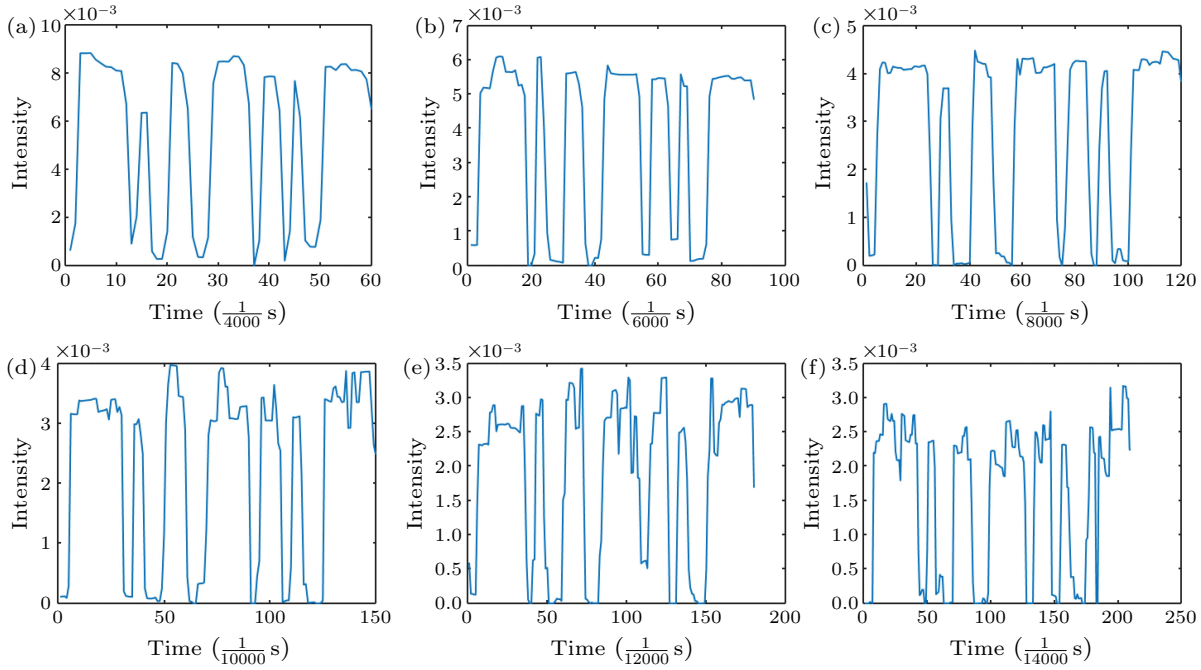


Fig. 7. Reconstructions of a 2 kHz random $0/1$ binary signal without normalization under modulation frequencies (a) 4 kHz, (b) 6 kHz, (c) 8 kHz, (d) 10 kHz, (e) 12 kHz, and (f) 14 kHz.

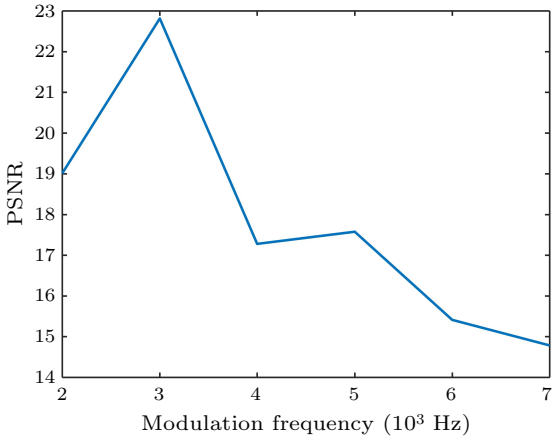


Fig. 8. PSNR versus modulation frequency in the numerical simulation experiment.

Table 1. The PSNR of results reconstructed from different dynamic detecting ranges.

Gray scale	8 bit	10 bit	12 bit	14 bit
PSNR	44.76	59.95	63.59	78.63

A numerical simulation has been performed to show the relation between the PSNR and the dynamic range of the detector, in which the time object was 100 bits $0/1$ binary signal, the $F_{\mathrm{M}}/F_{\mathrm{X}}$ is 3, and the number of measurements was 2048. Table 1 shows that high dynamic detecting range detector gives a better performance. To effectively restore a temporal signal with enhanced speed, an array detector boasting both a high dynamic range and swift response is imperative. Additionally, DMD technology can be advantageously substituted with more rapid modulation devices, for instance, spinning masks.

5. Conclusion

In summary, we have experimentally demonstrated single-shot TGI based on DMD and $+1/-1$ binary modulation, which is achieved by displaying a $0/1$ pattern with its inverse in one measurement. The high modulation speed of DMD and $+1/-1$ binary modulation acquire high SNR in fast nonperiodic temporal signal detection results. Some factors that contribute to the reconstructions are discussed. We believe that this single-shot TGI configuration could be valu-

able in many real applications.

Acknowledgment

Project supported by Beijing Institute of Technology Research Fund Program for Young Scholars (Grant No. 202122012).

References

[1] Todd B P, Shih Y H, Dmitry V S and Alexander V S 1995 *Phys. Rev. A* **52** R3429(R)
[2] Gatti A, Brambilla E, Bache M and Lugiato L A 2004 *Phys. Rev. Lett.* **93** 093602
[3] Valencia A, Scarcelli G, Mil D A and Shih Y H 2005 *Phys. Rev. Lett.* **94** 063601
[4] Zhang M H, Wei Q, Shen X, Liu Y F, Liu H L, Cheng J and Han S S 2007 *Phys. Rev. A* **75** 021803(R)
[5] Liu X F, Chen X H, Yao X R, Yu W K, Zhai G J and Wu L A 2014 *Opt. Lett.* **39** 2314
[6] Cheng J 2009 *Opt. Express* **17** 7916
[7] Meyers R E, Deacon K S and Shih Y H 2011 *Appl. Phys. Lett.* **98** 111115
[8] Basano L and Ottonello P 2006 *Appl. Phys. Lett.* **89** 091109
[9] Liu H L and Han S S 2008 *Opt. Lett.* **33** 824
[10] Deng C J, Gong W L and Han S S 2016 *Opt. Express* **24** 25983
[11] Chen X H, Kong F H, Fu Q, Meng S Y and Wu L A 2017 *Opt. Lett.* **42** 5290
[12] Zhang A X, He Y H, Wu L A, Chen L M and Wang B B 2018 *Optica* **5** 374
[13] Juan S T G, Luana O, Luke P, Vittorio C, Antonio C, Jacob T, Robyn T, Alessia P and Marco P 2020 *Optica* **7** 186
[14] Li M Q, Lan R M, Liu X F, Yao X R and Zhai G J 2020 *Appl. Phys. Lett.* **117** 084102
[15] Tomohiro S, Tero S and Ari T F 2010 *J. Opt. Soc. Am. B* **27** 2549
[16] Cho K and Noh J 2012 *Opt. Commun.* **285** 1275
[17] Ryczkowski P, Margaux B, Friberg A T, Dudley J M and Genty G 2015 *Nat. Photon.* **10** 167
[18] Xu Y K, Sun S H, Liu W T, Tang G Z, Liu J Y and Chen P X 2018 *Opt. Express* **26** 99
[19] Meng W W, Shi D F, Yuan K, Zha L B, Huang J, Wang Y J and Fan C Y 2020 *Opt. Lasers Eng.* **134** 106294
[20] Huang H H, Hu C Y, Yang S G, Chen M H and Chen H W 2020 *IEEE Photon. J.* **12** 1
[21] Wu H, Ryczkowski P, Friberg A T, Dudley J M and Genty G 2019 *Optica* **6** 902
[22] Jin M Y, Qian Z Y, Chen X W, Cui X G, Jiang K, Sun X J, Li D and Tian P F 2021 *Chin. Opt. Lett.* **19** 110602
[23] Chen X H, Jin M Y, Fu Q, Chen H L, Wang Y P, Qiu P J, Cui X G, Sun B Q and Tian P F 2021 *Opt. Lett.* **46** 1938
[24] Wang Y P, Jiang W J, Chen H l, Chen X W, Gao Y, Tian, P F and Sun B Q 2022 *J. Light Technol.* **40** 5426
[25] Fabrice D, Paul A M, Séverine D and Eric L 2016 *Optica* **3** 698
[26] Yu W K, liu X F, Yao X R, Wang C, Zhai Y and Zhai G J 2014 *Sci. Rep.* **4** 5834
[27] Candes E J and Wakin M B 2008 *IEEE Signal Process. Mag.* **25** 21
[28] Donoho D 2006 *IEEE Trans. Inform. Theory* **52** 1289
[29] Li C B 2011 *An efficient algorithm for total variation regularization with applications to the single pixel camera and compressive sensing* (MS thesis) (Houston: Rice University)